EurJIC
European Journal of Inorganic Chemistry

Research Article
doi.org/10.1002/ejic.202300620

Chemistry Europe
European Chemical Societies Publishing

www.eurjic.org

Luminescent Platinum(II) Complexes with a Tridentate Caffeine-Based NHC-Pincer Ligand: Synthesis, Electrochemistry and Photophysics

Oliver Bysewski,[a, b] Niklas Klosterhalfen,[c, d] Rose Jordan,[e] Lukas Kletsch,[e] Andreas Winter,[a, b] Axel Klein,[e] Benjamin Dietzek-Ivanšić,[c, d] and Ulrich S. Schubert*[a, b]

A strategy of "greening up" Pt(II) luminophores is presented. For this purpose, caffeine, as a renewable alkaloid and precursor for an *N*-heterocyclic carbene (NHC), is incorporated into a tridentate, pincer-type ligand framework. A series of luminescent Pt(II) complexes, containing the tridentate *bis*-NHC ligand and an arylacetylide ligand is reported. The complexes' electrochemistry and photophysics strongly depend on the electronic nature of the substituent on arylacetylide ligand. The use of bio-derived ligands represents one important approach to make emitters or sensitizers eco-friendlier by coming back to cheap, abundant and non-harmful staring materials for their synthesis.

Introduction

Platinum(II) complexes possess remarkable properties which have inspired intense research on such compounds and a manifold of applications has been proposed or even realized. This holds particularly true for the chemotherapeutic treatment of cancer by cisplatin, which was invented in the 1960s,[1–2] and the wide range of platinodrugs presented thereafter.[3–6] Aside from the medicinal application of Pt(II) compounds, their photophysical properties have been explored regarding a potential use as sensitizers for photovoltaics[7–10] or as emitters for organic light-emitting devices (OLEDS).[11–13] In the same context, notable achievements in the fields of non-linear optics,[14] catalysis,[15] photocatalysis (*e.g.*, hydrogen-evolution reaction),[6,16] and fabrication of alloy nanoparticles[17] have been made.

The enormous interest in *inter-alia* Pt(II) complexes for opto-electronic applications is due to the possibility to reach very high quantum yields of emission. Representing a heavy-metal ion, the efficient spin-orbit coupling enables fast intersystem crossing (ISC) after photo-excitation and, thus, singlet as well as triplet excitons can be harvested. As a result, theoretical quantum yields of up to 100% might be reached.[18–20] It has been demonstrated that by choosing a proper ligand set, the photophysical properties can be varied over a wide range. The Pt(II) center, representing a species of d^8 electron configuration, will adopt a square-planar coordination geometry. In many complexes, chelating ligands of the polypyridyl family are used to saturate two (*e.g.*, bidentate 2,2-bipyridine) or three coordination sites (*e.g.*, tridentate 2,2′:6′,2″-terpyridine).[6] In particular, cyclometalating variants of these ligands, in which at least one of the pyridine rings is replaced by a phenyl one, have attracted the most notable attention – complexes with quantum efficiency close to unity have been reported.[12–13,21–25]

Regarding the ancillary or co-ligands, σ-arylacetylides, as carbon-based ligands, have widely been used. The outstanding role of these anionic ligands is mainly due to the remarkably high stability of the Pt–C bond against moisture, air and temperature in concert with the typical ease-of-synthesis.[8,26–27] However, also other types of monodentate ligands have been employed, as co-ligands, to moderate the luminescence properties of Pt(II) complexes: Cyclometalated aryl or carboranyl moieties,[28–31] triphenyl pnictogens,[32] *etc.*. In recent years, *N*-heterocyclic carbenes (NHCs) have emerged as powerful ligands whose σ-binding strength is at least similar to those of phosphine ligands; unlike the latter, the Pt–NHC linkages features an overall superior stability, which is favorable for many applications.[33] Not only in the context of medicinal

[a] *O. Bysewski, Dr. A. Winter, Prof. Dr. U. S. Schubert*
Laboratory of Organic and Macromolecular Chemistry (IOMC)
Friedrich Schiller University Jena
Humboldtstr. 10, 07743 Jena, Germany
E-mail: ulrich.schubert@uni-jena.de

[b] *O. Bysewski, Dr. A. Winter, Prof. Dr. U. S. Schubert*
Center for Energy and Environmental Chemistry Jena (CEEC Jena)
Friedrich Schiller University Jena
Philosophenweg 7a, 07743 Jena, Germany

[c] *N. Klosterhalfen, Prof. Dr. B. Dietzek-Ivanšić*
Institute for Physical Chemistry (IPC)
Friedrich Schiller University Jena
Helmholtzweg 4, 07743 Jena, Germany

[d] *N. Klosterhalfen, Prof. Dr. B. Dietzek-Ivanšić*
Research Department Functional Interfaces
Leibniz Institute of Photonic Technology (Leibniz-IPHT)
Albert-Einstein-Str. 9, 07745 Jena, Germany

[e] *R. Jordan, L. Kletsch, Prof. Dr. A. Klein*
Institute for Inorganic Chemistry, Department of Chemistry and Biochemistry, Faculty of Mathematics and Natural Sciences University of Cologne
Greinstr. 6, 50939 Cologne, Germany

Supporting information for this article is available on the WWW under https://doi.org/10.1002/ejic.202300620

Research Article
doi.org/10.1002/ejic.202300620

chemistry,[34–36] but also with respect to opto-electronic applications Pt(II) complexes with NHC ligands have been studied.[37] In this respect, the NHC moiety might either represent a monodentate ligand[35,38] or be a part of a bidentate,[39–43] tridentate[44–45] or even tetradentate ligand framework.[46–47]

In the overwhelming majority of the published studies imidazole or one of its derivatives (*e.g.*, benzo[*d*]imidazole) is employed as the NHC precursor. In addition to these, mesoionic carbenes, derived from triazolium salts, represent a (still) less frequently used alternative.[44,48–49] However, none of these systems fulfills the "12 criteria of green chemistry", which have been defined by Anastas and Warner;[50] indeed, the mostly multi-step synthesis relies on non-renewable sources, *i.e.*, products from the petrochemical industry.[51–52] Xanthines, on the other hand, are naturally occurring alkaloids, which allow for a more sustained and eco-friendlier NHC synthesis *via* straightforward derivatization.[53] According to the statistics of the worldwide coffee market, *ca.* 166.63 Mio bags, each with 60 kg of coffee beans, were sold in 2020/21.[54] Caffeine and theophylline can be isolated from the respective plant material by extraction with supercritical CO_2 and subsequent ion-exchange chromatography using water at various pH values, as the eluent.[55–58] Thus, the starting material is readily available and can be used even for large-scale synthesis. As summarized by Morales-Morales *et al.*, a wide range of organometallic compounds incorporating xanthine-derived NHCs has already been reported.[59] Most of these studies were devoted to biomedical applications. More recently, such complexes have also been employed as catalysts in various organic reactions: Hydrogenation of ketones,[60] cross-coupling reactions,[61–63] and Diels-Alder reactions.[64]

On the other side, studies dealing with luminescent Pt(II) complexes with xanthine-derived NHC ligands are exceedingly rare. For example, the 1,3,7,9-tetramethylxanthinium cation was used, as a precursor, for the synthesis of Pt(II) complexes with one NHC ligand.[65–66] In previous work, we reported the synthesis and structural characterization of complexes **2** and **3**, which contained a CNC coordinating tridentate, *bis*-NHC ligand (Figure 1a).[67] The ligand design allowed, due to the CH_2 bridges, for an almost ideal square-planar coordination geometry (Figure 1b). Pd(II) complex **3** displayed a remarkably high catalytic activity in various cross-coupling reactions – even at low catalyst loading in the ppm range.[61] In continuation of this work, we now turn back to the Pt(II) complex **2** and present a study of its arylacetylide complexes **4**–**8** (Scheme 1). Herein, we report their synthesis and structural characterization along with their basic electrochemical and optical properties, which are meaningful for their potential use as luminescent bio-mimetic molecules.

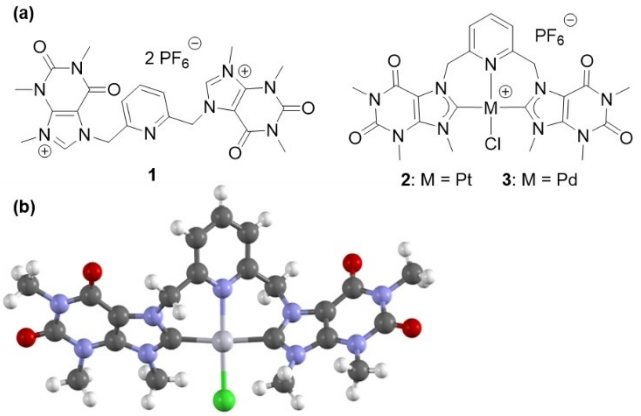

Figure 1. (a) Schematic representation of the protoligand 1 and its Pt(II) and Pd(II) complexes **2** and **3**. (b) Solid-state structure of **2** (counter ion and solvent molecules omitted for clarity).[67] Figure reproduced from the original data (CCDC entry no. 2157149) set using the Mercury 2022.3.0 software.[68]

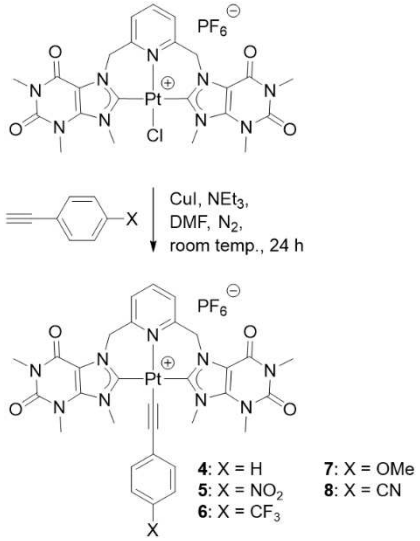

Scheme 1. Schematic representation of the synthesis of complexes **4** to **8**.

Results and Discussion

Synthesis and characterization

For the synthesis of complexes **4** to **8**, phenylacetylenes with different substituents in *para*-position were applied. The use of electron-withdrawing as well as -donating groups showcases the tunability of the photophysical and electrochemical properties of the derived complexes *via* the variation of the terminal moieties. Following the fundamental strategy for the cross-coupling between precursor complex **2** and the alkyne derivative, the starting materials were allowed to react in the presence of CuI, as catalyst, and NEt_3, as base for trapping the liberated HCl (Scheme 1).[69] Worth emphasizing, all reactions were run under inter conditions to counteract the Glaser-type homo-coupling of the respective phenylacetylenes. Even though substrate conversion was always quantitative, according to thin-layer chromatographic (TLC) analysis, the isolated yield varied between 29 and 92 %. The precipitation step afforded the complexes as very fine powders, which were difficult to collect.

All complexes were characterized by ^1H and ^{13}C nuclear magnetic resonance (NMR) spectroscopy as well as high-resolution electrospray-ionization mass spectrometry (HR-ESI-

MS). In neither case, single crystals suited for X-ray diffraction (XRD) analysis were obtained. The NMR spectra of **4** to **8** revealed only marginal differences in the signal positions. The ^{1}H NMR signals, which were assigned to the protons of the pyridine ring were located between 8.10 and 7.80 ppm. The characteristic signals of the CH_2 bridges, which were split up due to the diastereotopicity of the protons, were observed at ca. 6.50 and 5.40 ppm, respectively; for comparison, these signals appeared at 6.55 and 5.70 ppm in the case of the chloride complex **2**. Thus, a more pronounced shielding due to the presence of the arylacetylide moiety was assumed. The proton signals of the caffeine's CH_3 groups were unaffected by the terminal substituent; they were at fixed positions of 4.35, 3.77, and 3.33 ppm. Representatively, the ^{1}H NMR spectra of the protoligand (**1**), the chlorido complex (**2**) and the phenylacetylide complex (**8**) are depicted in Figure 2. The ^{13}C NMR signal of the NHC carbon atom was located at 173.3 and 172.0 ppm for complexes **2** and **4**, respectively. Within the series of arylacetylide complexes, there was only little deviation in the signal position, regardless of the electronic nature of the co-ligand. The ^{1}H and ^{13}C NMR spectra of complexes **4** to **8** are provided in the Supporting Information SI (Figures SI-1 to SI-11). The formation of the desired complexes was corroborated by high-resolution electrospray-ionization time-of-flight mass spectrometry (HR-ESI-TOF-MS). In all cases, the characteristic [M^+] peaks, whose isotopic patterns accurately matched those of the respective calculated ones, were observed ($\Delta m/z \leq 2.7$ ppm; Figure 3). The mass spectra of all complexes are provided in the SI, Figures SI-12 to SI-16.

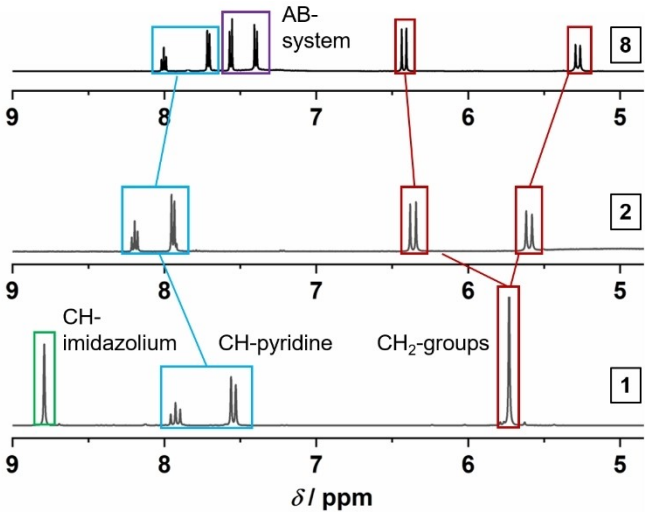

Figure 2. ^{1}H NMR spectra of compounds **1**, **2**, and **8** (from the bottom to top). All spectra were recorded in CD_3CN at 300 MHz and 25 °C. For clarity, only the most significant region from 5 to 9 ppm is shown.

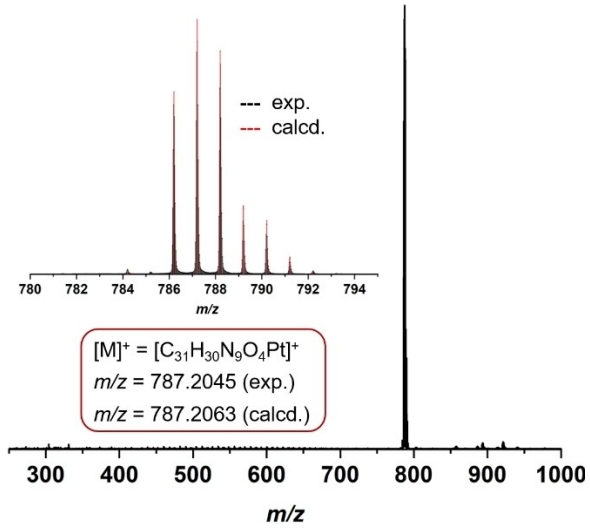

Figure 3. HR-ESI-TOF mass spectrum of complex **4**. The inset shows the comparison of the measured and calculated isotopic patterns of the [M]$^+$ peak.

Electrochemical properties

All complexes showed an irreversible first reduction wave in their cyclic voltammograms (CVs) at *ca.* −2 V *vs.* the ferrocene/ferrocenium (Fc/Fc^+) redox couple in THF or MeCN solution, which contained *n*-Bu_4NPF_6, as electrolyte. Representatively, the CVs of the complexes **2** and **7** are shown in Figure 4, selected data are summarized in Table 1 (the CVs of all complexes and protoligand **1** together with the full data can be found in the SI: Figures SI-17 to SI-21, Table SI-1). A slightly lower, *i.e.*, more negative, potential was found for the protoligand's first reduction at −2.16 V, which was followed by a second wave at −2.71 V (Figure SI-21). In addition to this, minor irreversible waves were observed for some of the Pt(II) complexes in the potential range from −2.1 to −2.5 V.

The NO_2-substituted complex **5** revealed a reversible first reduction at −1.61 V (Figure SI-18). Taking previous reports on related NO_2-substituted complexes into account, one can assign this process to the NO_2-centred reduction.[70–73] Remarkably, the singly reduced complex **5**$^-$ showed only a marginal cathodic

Table 1. Selected redox potentials of Pt(II) complexes **2** and **4** to **8**.[a]

Compound	E_{pc}^{red1} [b]	$E_{1/2}^{ox1}$ [c]	ΔE [d]
2	−1.99 −1.90 [e]	– 1.41 (irr) [e]	– 3.31
4	−2.02 −1.96 [e]	0.09 0.15 [e]	2.11
5	−2.06 [f]	0.18	2.24
6	−2.04	0.14	2.18
7	−2.03	0.17	2.20
8	−1.98	0.18	2.16
protoligand **1**	−2.16	1.01	3.17

[a] From cyclic voltammetry (CV) in THF, which contained 0.1 M *n*-Bu_4NPF_6; potentials are listed in V *vs.* Fc/Fc^+ with an accuracy of ±0.003 V. [b] E_{pc}^{red1}: Cathodic peak potential for an irreversible (irr) reduction. [c] $E_{1/2}^{ox1}$: Half-wave potential for a (partially) reversible oxidation. [d] $\Delta E = E_{1/2}^{ox1} - E_{pc}^{red1}$. [e] Measured in 1 M *n*-Bu_4NPF_6 in CH_3CN. [f] A first reversible wave at $E_{1/2} = -1.61$ is attributed to the reduction of the NO_2-group.

Research Article
doi.org/10.1002/ejic.202300620

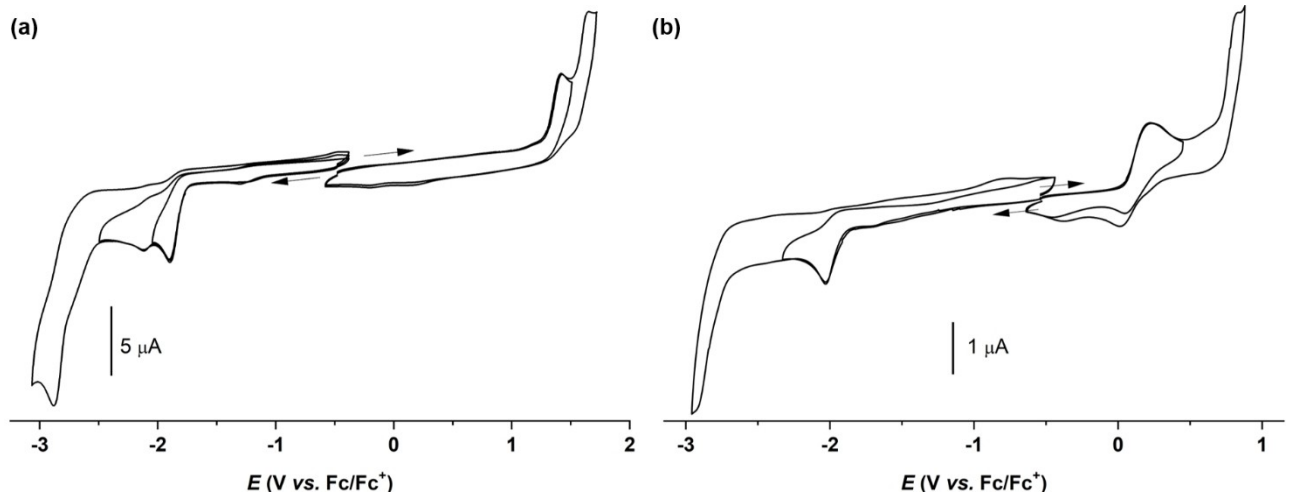

Figure 4. (a) Cyclic voltammograms of **2** in a 0.1 M solution of *n*-Bu_4NPF_6 in CH_3CN. (b) Cyclic voltammograms of **7** in a 0.1 M solution of *n*-Bu_4NPF_6 in THF. All measurements were conducted at 298 K and at a scan rate of 100 mV s^{-1}.

shift for its second reduction when compared to the other complexes of the series (*i.e.*, −2.06 V *vs.* −1.96 to −2.04 V).

The chlorido complex **2** did not show any oxidation wave up to the potential of 1.23 V, representing the discharge limit of THF, and was only sparsely soluble in this solvent. However, irreversible oxidation processes occurred at 1.41 and 1.61 V when the CV was recorded in a solution of *n*-Bu_4NPF_6 in CH_3CN. This finding contrasts the behavior of complexes **4** to **8**, which all revealed reversible oxidation waves in the range of 0.1 to 0.2 V in both THF and CH_3CN. These processes were accompanied by further irreversible oxidations at higher potentials between 0.8 and 1.1 V. The first oxidation potentials ($E_{1/2}^{ox1}$) of the arylacetylide complexes increases in the following order: **4** (X = H) < **6** (X = CF_3) < **7** (X = OMe) < **8** (X = CN) ≈ **5** (X = NO_2).

The electrochemical band gaps (ΔE) ranged from 2.11 to 2.24 V; while a ΔE value of 3.31 V was calculated for the chlorido complex **2**. As summarized in Table 1, the values of ΔE increase as follows: **4** < **8** < **6** < **7** < **5**. Interestingly, neither the series of the first oxidation potentials nor the trend in the evolution of the electrochemical band gaps did simply correlate with the expected electronic influence of the terminal substituent X.

The first reduction step can be assigned to a pyridine-centered process as it is, on first sight, highly invariant and does not depend much on the co-ligand. A closer look shows, that chloride as a weaker σ-donor, compared with an alkynyl moiety, in *trans*-position to the pyridine unit results in slightly easier reducibility, in line with this assignment. Due to their small size, the following reduction wave can be assigned to products, which resulted from the first reduction step and a subsequent chemical reaction (according to an *EC* mechanism).[74–75] This assignment is also in line with Wolf's recent report on the Pt(II) complexes **9**, which possessed either a chlorido or MeCN co-ligand (Figure 5).[76] For the Pt(II) complexes **10** with a *bis*-NHC ligand, *i.e.*, pyridine-2,6-bis-imidazolydene (Figure 5), significantly lower reduction potentials were found (*ca.* −1.3 V);[45,77] the reduction potential was almost invariant when comparing the complexes with either Cl^-, CN^-, or MeCN as the co-ligands.[77] This is completely in line with our findings for **2** when compared with **4** to **8**.

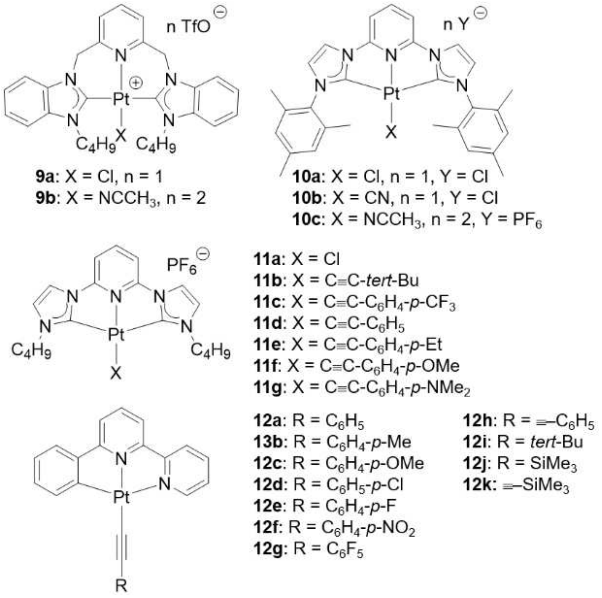

Figure 5. Schematic representation of the Pt(II) complexes **9**–**12**.

As an oxidation process at low potential is absent for the chlorido complex **2**, oxidation of complexes **4** to **8** can be attributed to the arylacetylide group. In similar Pt(II)–NHC complexes with arylacetylide ligands (**11**, Figure 5), such oxidation processes were observed in the potential range from 0.12 to 1.26 V, depending on the ligand's structure.[77–78] Also the closely related CNN cyclometalated complexes **12** (Figure 5) revealed very similar potentials ranging from 0.04 to 0.29 V.[79] Interestingly, in in the aforementioned cases, these oxidations were of irreversible nature;[77–79] whereas, a reversible behavior was found for **4** to **8**. It is assumed that contributions from the Pt(II) center[77] accounted for the observed reversibility of the oxidation.

Research Article
doi.org/10.1002/ejic.202300620

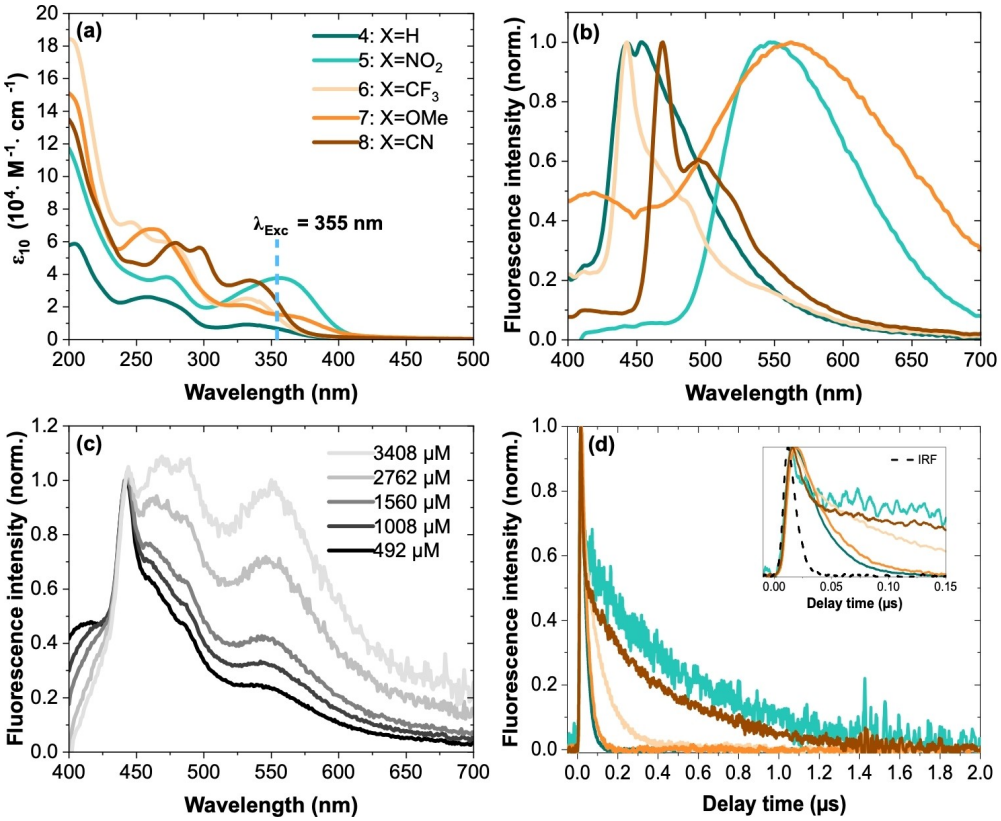

Figure 6. Absorption (a) and emission (b) spectra of complexes **4** to **8** measured in CH_3CN at 298 K. Emission and transient emission data were collected upon excitation of the complexes at 360 and 355 nm, respectively. (c) Concentration-dependent emission of compound **6** under the conditions mentioned above (normalized to the emission at 443 nm). (d) Transient emission traces recorded under the same conditions. The fast decay component of **5**, **6**, and **8** is visible in the sub 50 ns region, displayed in the inset along with the instrument response function (IRF).

Photophysical properties

The electronic absorption spectra of complexes **4** to **8**, which are depicted in Figure 6a, revealed several distinct absorption bands at wavelengths below 400 nm. With reference to previous studies on alkynyl Pt(II) and phenylalkynyl Pt(II) complexes containing CNC-type pincer ligands,[80] we assign the high-energy absorption bands between 240 and 310 nm to intraligand $\pi\rightarrow\pi^*$ transitions. The lower-energy transitions centered in the range from 310 to 400 nm are assigned to a mixture of intraligand and metal-to-ligand charge transfer transitions (ILCT and MLCT). These assignments are supported by TD-DFT calculations (for details, see the Experimental Section). Figure 7 shows the TD-DFT calculated absorption spectrum for **4** with transition-difference densities for selected transitions. Remarkably, TD-DFT consistently vastly overestimates the intensity of the HOMO-LUMO transition, which appears only weakly in the experimental spectra and features major MLCT character into the central pyridine ring Detailed information on the predicted character of the calculated transitions is given in Table SI-2.

The emission spectra recorded upon excitation of these ILCT/MLCT transitions are presented in Figure 6b. While complexes **5** and **7** have broad and structureless bands, centered around 547 and 562 nm, respectively, complexes **4**, **6**, and **8** display hypsochromically shifted emission, in which (at least) two distinct emission bands are visible. In general, the complexes are only weakly emissive with quantum yields below 1% (Table 2). This is in accordance with other phenylalkynyl Pt(II) complexes in solution (although values of up to 93% were observed for the same complexes when excited as dry powders).[80] The complexes were also processed into thin-solid films using poly(methyl methacrylate) (PMMA), as the matrix polymer. The spin-coated films showed an apparent increase in

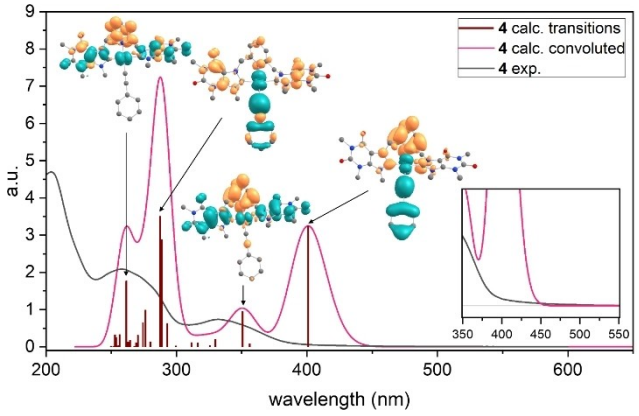

Figure 7. TD-DFT calculated UV/vis absorption spectrum for **4** compared to the experiment with transition difference densities for selected transitions.

Research Article
doi.org/10.1002/ejic.202300620

Table 2. Photophysical properties of Pt(II) phenylacetylide complexes in solutions of CH_3CN at 298 K.[a]

Compound	E_{em} (eV)	Φ_{ph}	τ_1 (ns)	τ_2 (ns)
4	2.74	< 1%	1.9	20.9
5	2.27	< 1%	25.7	552.1
6	2.80	< 1%	4.6	82.6
7	2.21	< 1%	2.5	26.7
8	2.64	< 1%	21.6	443.1

[a] E_{em}: emission maxima; Φ_{ph}: photoluminescence quantum yields, τ_1 and τ_2: excited states lifetimes from a biexponential decay fit. Data recorded upon irradiation at $\lambda = 355$ nm.

emission intensity, which, due to the inhomogeneity of the samples, could not be quantified.

One possible interpretation for these results obtained in solution is a substituent-dependent emission of either the excited monomer (sharp emission at ca. 450 nm) or excimer formation (broad emission at longer wavelengths).[43] Following this assumption, the monomer emission is tentatively assigned to an admixture of ILCT and MLCT states,[78] which are most likely of triplet character considering the long emission lifetimes (Table 2). In order to test this theory, concentration-dependent measurements of complex **6** were performed. When the concentration of this compound in solution is increased, the emission intensity of the monomer emission is reduced in comparison to the excimer emission at 550 nm (Figure 6c). At the same time, the overall emission quantum yield decreases, likely due to self-quenching without excimer formation. Similar results were also found for other NHC-containing alkynyl Pt(II) compounds in PMMA films.[78] The absence of low-energy bands in the UV-vis absorption spectra upon increasing the concentration corroborates the assumption that excimers rather than ground-state dimers were formed (Figure SI-22).

While excimer formation can be induced for complex **6** by increasing its concentration in solution, the same process can also be suppressed for complexes **5** and **7** by immobilizing them in solvent glasses. The emission measurements, which were conducted for all complexes at 80 K, provided increased emission intensities than at room temperature in solution. Raising the temperature back to 160 K allowed the complexes to be mobile again and, thus, their emission intensity decreased (Figure SI-23). In all cases, the emission profile at 80 K was sharper and more structured (representatively, the emission spectra of 6 at 80 K and room temperature is depicted in Figure 8a). Moreover, the emission band of **5** and **7** also experiences a blue shift with decreasing temperature; this indicates that "monomers" are indeed formed at low temperatures (Figure 8b). Interestingly, the emission at 160 K does not follow this trend; this is associated with the used CH_3CN/CH_2Cl_2 solvent mixture, which freezes at this point. A summary of all emission spectra, recorded at 80 K is given in Figure SI-23.

At last, the red-edge effect observed in the parent complex **2**[67] was not visible for any of the complexes **4** to **8** upon variation of the excitation wavelength from 260 to 380 nm (Figure SI-24). This leads us to presume, that the low-energy emission indeed stems from an excimer rather than a ground-state dimer.

Closer inspection of the data reveals no direct correlation between the position or intensity of the electronic absorption and emission spectra and the electron-donating or -withdrawing effect of the various substituents. While bathochromic emission shifts have previously been observed for NCN Pt(II) complexes with electron-donating amino substituents,[81] this does not provide an explanation for the occurrence of the same effect for both methoxy and nitro in this context. As discussed above, the long emission lifetime indicates the presence of phosphorescence in **4** to **8** (Figure 6d). Particularly for compounds **5** and **8**, emission lifetimes of several hundreds of nanoseconds were observed (Table 2) in addition to a (faster) decay component, which was found for complexes **5**, **6**, and **8**. A similar biexponential decay behavior was also seen for related Pt(II) complexes.[80,82]

Fitting the experimental data with two decay components yielded the lifetimes as listen in Table 2. Details on the deconvolution process and the fit results can be found in the SI (Figure SI-25).

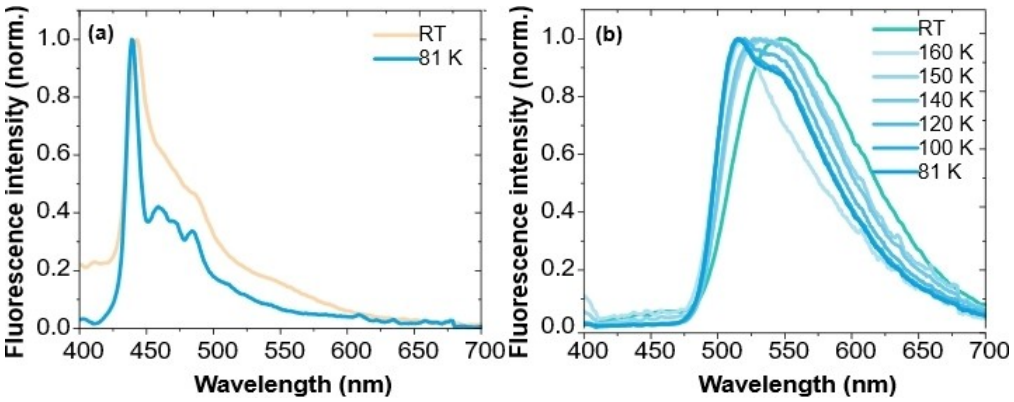

Figure 8. (a) Emission spectra of complex **6** at 80 K and room temperature. (b) Evolution of the emission properties of complex **5** upon gradual warming from 80 K to room temperature (all measurements were performed in a CH_3CN/CH_2Cl_2 1:1 mixture).

Research Article
doi.org/10.1002/ejic.202300620

Conclusions

A series of Pt(II) complexes bearing a tridentate NHC-pincer and alkyne co-ligands has been prepared. These complexes have been studied regarding their electrochemical and photophysical characteristics. These studies corroborated a profound influence of the lateral substituents on their properties in solution.

In UV-vis absorption experiments both intraligand and charge transfer (ILCT and MLCT) transitions are observed. Upon excitation of the latter, pronounced excimer formation is assumed for complexes **5** and **7** on the basis of red-shifted and structureless emission bands. This behavior is also found for complex **6**, though only at elevated concentrations. However, ground-state association can be ruled out due to the invariance of the emission spectra on the excitation wavelength and the absence of low-energy absorption bands upon increase of the concentration. At lower concentrations, complexes **4**, **6**, and **8** are assumed to undergo phosphorescence decay from states with ILCT or MLCT character.

Experimental Section

All reagents and analytical-grade solvents were purchased from commercial suppliers and used as received. Protoligand **1** and Pt(II) complex **2** were synthesized following the procedure published beforehand.[67] In all cases, the reaction mixtures were purged with N_2 for 20 min before starting the reactions. ^{1}H and ^{13}C NMR spectra were recorded at 25 °C on Bruker AVANCE instruments (250, 300 or 500 MHz) in deuterated solvents (Eurisotop). Chemical shifts are given in ppm and referenced to the solvent signal. High-resolution electrospray ionization time-of-flight mass spectrometry (HR-ESI-TOF-MS) was performed on an ESI-(Q)-TOF-MS MICROTOF II (Bruker Daltonics GmBH & Co KG) mass spectrometer.

Steady-state absorption measurements were performed in 1 cm quartz cells and recorded with a V-760 (JASCO) spectrophotometer. Fluorescence emission spectra were acquired using a FLS980 emission spectrophotometer (Edinburgh Instruments) with a Xenon lamp (ozone free, 450 W) as white light source. Fluorescence quantum yields and low-temperature measurements were performed in the same device using either an Ulbricht integrating sphere or an OptistatDN cryostate (Oxford Instruments), which was cooled with liquid nitrogen. Fluorescence lifetimes were acquired in 1 cm quartz cells under ambient conditions using a custom-built Nd:YAG laser setup with a 10 Hz repetition rate (Pascher Instruments). Details on the experimental setup can be found elsewhere.[83]

Electrochemical measurements were carried out in 0.1 M n-Bu_4NPF_6 solution in THF or CH_2Cl_2 at 298 K and at a scan rate of 100 mV s^{-1}. A three-electrode configuration (*i.e.*, glassy-carbon working electrode, Pt counter electrode, Ag/AgCl pseudo-reference electrode) and an Autolab PGSTAT30 or an μStat400 potentiostat (Metrohm) were used. The potentials were referenced against the ferrocene/ferrocenium (Fc/Fc^+) redox couple as internal standard.

Computational details

DFT calculations were performed using ORCA 5.0.2.;[84–85] def2 TZVP basis sets were used for all atoms as well as the corresponding def2-ECP for Pt.[86] The geometries of **4** as well as of **2**, for method cross-validation, were optimized at the BP86 level of theory, using Grimme's D3 dispersion correction and the conductor-like polarizable continuum model (CPCM), which is parametrized for CH_3CN as an approximate solvation model.[87–92] The geometry optimizations were followed up with numerical frequency calculations in order to confirm the energetic minimum nature of the optimized structure, as indicated by the absence of imaginary modes. On the optimized geometries, single-point and TD-DFT calculations were performed using the B3LYP functional, Grimme's D3 dispersion correction and CPCM parametrized for THF, as the solvent.[87,93–94] For the TD-DFT calculations of the absorption spectra, 30 roots (transitions) for singlets and triplets each were included for each complex. Broadened spectra were obtained using the orca_mapspc module with 2000 cm^{-1} full-width at half-maximum band broadening. Orbital isosurfaces and TD-DFT difference densities were extracted from the single point calculations using the ORCA module orca_plot and plotted with the visualization software CHEMCRAFT at an isovalue of 0.04 for molecular orbitals and 0.001 for difference densities.[95]

General procedure for the synthesis of arylacetylide complexes

An excess of the respective arylacetylene and Pt(II) complex **2** (1.0 eq) were dissolved in a large amount of DMF (20 mL). Then cuprous iodide (1.5 eq) and triethylamine (2 mL) were added successively and the reaction mixture stirred vigorously at room temperature for 24 h. The mixture was filtered and the solvent was evaporated under reduced pressure. The residue was dissolved in a minimum amount of DMF and added to large excess of diethyl ether. The resulting precipitate was filtered off, washed three times with toluene and dried *in vacuo* to afford the product as a colored solid.

Complex 4

The reaction of **2** (12 mg, 0.027 mmol), phenylacetylene (0.1 mL) and CuI (2 mg, 0.042 mmol)) afforded a yellow solid (6 mg, 45 %).

^{1}H NMR (CD_3CN, 300 MHz, 25 °C): δ = 8.07 (t, 1H, J = 7.8 Hz, H^a), 7.79 (d, 2H, J = 7.8 Hz, H^b), 7.36 (m, 2H, H^9), 7.29 (m, 2H, H^{10}), 7.21 (m, 1H, H^X), 6.50 (d, 2H, J = 15.3 Hz, H^c), 5.37 (d, 2H, J = 15.3 Hz, H^c), 4.38 (s, 6H, H$^{9'}$), 3.76 (s, 6H, H$^{1'}$), 3.33 ppm (s, 6H, H$^{3'}$); ^{13}C NMR (CD_3CN, 125 MHz, 25 °C): δ = 173.3 (C^{carbene}, 155.2 (C$^{4/5}$), 155.1 (C$^{5/4}$), 152.2 (C^1), 143.0 (C^a), 142.5 (C^3), 132.5 (C^b), 129.6 (C^9), 128.6 (C^8), 127.7 (C^X), 127.4 (C^{10}), 109.9 (C^2), 109.6 (C^6), 71.3 (C^7), 53.7 (C^c), 53.9 (C^c), 40.1 (C$^{9'}$), 33.1 (C$^{3'}$), 29.2 ppm (C$^{1'}$); HR-ESI-MS: calcd. for $[C_{31}H_{30}N_9O_4Pt]^+$ m/z = 787.2063, found 787.2045 [M$^+$].

Complex 5

The reaction of **2** (12 mg, 0.027 mmol), 4-nitrophenylacetylene (50 mg) and CuI (20 mg, 0.042 mmol)) yielded a yellow solid (6 mg, 43 %). ^{1}H NMR (CD_3CN, 300 MHz, 25 °C): δ = 8.07 (t, 1H, J = 7.8 Hz, H^a), 7.79 (d, 2H,J = 7.8 Hz, H^b), 7.36 (m, 2H, H^9), 7.29 (m, 2H, H^{10}), 7.21 (m, 1H, H^X), 6.50 (d, 2H, J = 15.3 Hz, H^c), 5.37 (d, 2H, J = 15.3 Hz, H^c), 4.38 (s, 6H, H$^{9'}$), 3.76 (s, 6H, H$^{1'}$), 3.33 ppm (s, 6H, H$^{3'}$); ^{13}C NMR (CD_3CN, 125 MHz, 25 °C): δ = 172.9 (C^{carbene}), 155.2 (C$^{4/5}$), 155.1 (C$^{5/4}$), 152.1 (C^1), 146.9 (C^X), 143.0 C^a), 142.5 (C^3), 135.5 (C^8) 133.2 (C^9), 128.6 (C^8), 127.4 (C^b), 124.8 (C^{10}), 109.9 (C^2), 109.6 (C^6), 71.3 (C^7), 53.7 (C^c), 53.9 (C^c), 40.1 (C$^{9'}$), 33.1 (C$^{3'}$), 29.2 ppm (C$^{1'}$); HR-ESI-MS: calcd. for $[C_{31}H_{29}N_{10}O_6Pt]^+$ m/z = 832.1907, found 832.1916 [M$^+$].

Complex 6

The reaction of **2** (12 mg, 0.027 mmol), 4-trifluoromethane-phenylacetylene (0.05 mL) and CuI (2 mg, 0.042 mmol)) afforded a yellow

solid (4 mg, 29%). ^{1}H NMR (CD_3CN, 300 MHz, 25 °C): δ = 8.08 (t, 1H, J = 7.8 Hz, H^a), 7.78 (d, 2H, J = 7.8 Hz, H^b), 7.59 (m, 2H, H$^{9/8}$), 7.56 (m, 2H, H$^{8/9}$), 6.52 (d, 2H, J = 15.3 Hz, H^c), 5.47 (d, 2H, J = 15.3 Hz, H^c), 4.37 (s, 6 H, H$^{9'}$), 3.77 (s, 6H, H$^{1'}$), 3.33 ppm (s, 6H, H3′); ^{13}C NMR (CD_3CN, 125 MHz, 25 °C): δ = 172.7 (C^{carbene}), 155.2 (C$^{4/5}$), 155.1 (C$^{5/4}$), 152.2 (C^1), 143.2 (C^a), 142.5 (C^3), 133.1 (C^{10}), 132.6 (C^8), 128.4 (C^9), 127.4 (C^b), 126.4 (CF_3), 109.9 (C^2), 108.3 (C$^{6\&7}$), 83.2 (C^c), 53.8 (C^c), 48.2 (C^c), 40.3 (C$^{9'}$), 33.3 (C$^{3'}$), 29.2 ppm (C$^{1'}$); HR-ESI-MS: calcd. for $[C_{32}H_{29}F_3N_9O_4Pt]^+$ m/z = 855.1937, found 855.1916 [M$^+$].

Complex 7

The reaction of **2** (12 mg, 0.027 mmol), 4-methoxy-phenylacetylene (50 mg) and CuI (2 mg, 0.042 mmol) yielded a yellow solid (11 mg, 79%). ^{1}H NMR (CD_3CN, 300 MHz, 25 °C): δ = 8.07 (t, 1H, J = 7.8 Hz, H^a), 7.78 (d, 2H, J = 7.8 Hz, H^b), 7.30 (m, 2H, H$^{9/8}$), 6.84 (m, 2H, H$^{8/9}$), 6.50 (d, 2H, J = 15.3 Hz, H^c), 5.37 (d, 2H, J = 15.3 Hz, H^c), 4.39 (s, 6 H, H$^{9'}$), 3.77 (s, 6H, H$^{1'}$), 3.33 ppm (s, 6H, H$^{3'}$); ^{13}C NMR (CD_3CN, 125 MHz, 25 °C): δ = 173.3 (C^{carbene}), 155.2 (C$^{4/5}$), 159.7 (C^X) 155.2 (C$^{5/4}$), 155.1 (C$^{4/5}$) 152.1 (C^1), 142.9 (C^a), 142.4 (C^3), 133.8 (C^{10}), 127.4 (C^b), 120.9 (C^8), 119.4 (C^9), 115.1 (C^2), 109.5 (C^6), 83.2 (C^7), 53.8 (C^c), 53.7 (C^{OMe}) 53.7 (C^c), 40.1 (C$^{9'}$), 33.1 (C$^{3'}$), 29.2 ppm (C$^{1'}$); HR-ESI-MS: calcd. for $[C_{32}H_{32}N_9O_5Pt]^+$ m/z = 817.2171, found 817.2151 [M$^+$].

Complex 8

The reaction of **2** (12 mg, 0.027 mmol), 4-cyanophenylacetylene (0.05 mL) and CuI (2 mg, 0.042 mmol)) afforded a yellow solid (12 mg, 92%). ^{1}H NMR (CD_3CN, 300 MHz, 25 °C): δ = 8.09 (t, 1H, J = 7.8 Hz, H^a), 7.81 (d, J = 7.8 Hz, H^b), 7.65 (m, 2H, H$^{8/9}$), 7.48 (m, 2H, H$^{9/8}$), 6.52 (d, 2H, J = 15.3 Hz, H^c), 5.37 (d, 2H, J = 15.3 Hz, H^c), 4.35 (s, 6 H, H$^{9'}$), 3.77 (s, 6H, H$^{1'}$), 3.33 ppm (s, 6H, H$^{3'}$); ^{13}C NMR (CD_3CN, 125 MHz, 25 °C): δ = 172.9 (C^{carbene}), 155.2 (C/$^{4/5}$), 155.1 (C$^{5/4}$), 152.1 (C^1), 143.2 (C^a), 142.5 (C^3), 133.4 (C^9), 133.3 (C^8), 133.2 (C^{10}), 127.4 (C^b), 120.2 (C^X), 110.2 (C^{CN}), 109.6 (C^2), 108.9 (C^6), 86.2 (C^7), 53.7 (C^c), 40.1 (C$^{9'}$), 33.2 (C$^{3'}$), 29.2 ppm (C$^{1'}$); HR-ESI-MS: calc for $[C_{32}H_{29}N_{10}O_4Pt]^+$ m/z = 812.2016, found 812.2006 [M$^+$].

Supporting Information

The authors have cited an additional reference within the Supporting Information (SI).[96] The SI contains the ^{1}H and ^{13}C NMR as well as the high-resolution ESI mass spectra of the complexes **4** to **8**. Furthermore, the full cyclic voltammograms and tabulated redox potentials of all compounds can be found in the SI. The excitation wavelength dependent emission and transient emission decay data of **4** to **8** are also shown.

Acknowledgements

The authors thank Rica Patzschke and Nicole Fritz for their support in recording the NMR and HR-ESI-MS spectra, respectively. Financial support by the Deutsche Forschungsgemeinschaft (DFG) within the Priority Program "Light-controlled reactivity of metal complexes" is kindly acknowledged (SPP2102-LCRM; grant numbers SCHU 1229/16-1 and 62-1, KL 1194/16-1 and 16-2 as well as DI 1517/31-1 and 19-1). Open Access funding enabled and organized by Projekt DEAL.

Conflict of Interests

The authors declare no conflict of interest.

Data Availability Statement

The data that support the findings of this study are available from the corresponding author upon reasonable request.

Keywords: alkyne ligands · electrochemistry · luminescence · photophysics · platinum

[1] B. Rosenberg, L. Van Camp, T. Krigas, *Nature* **1965**, *205*, 698–699.
[2] W. I. Rosenblum, *Circ. Res.* **1969**, *24*, 887–892.
[3] D. Lebwohl, R. Canetta, *Eur. J. Cancer* **1998**, *34*, 1522–1534.
[4] I. Kostova, *Recent Pat. Anti-Cancer Drug Discovery* **2006**, *1*, 1–22.
[5] U. Ndagi, N. Mhlongo, M. E. Soliman, *Drug Des. Dev. Ther.* **2017**, *11*, 599–616.
[6] I. Eryazici, C. N. Moorefield, G. R. Newkome, *Chem. Rev.* **2008**, *108*, 1834–1895.
[7] L. Xu, H.-B. Yang, *Chem. Rec.* **2016**, *16*, 1274–1297.
[8] A. Haque, L. Xu, R. A. Al-Balushi, M. K. Al-Suti, R. Ilmi, Z. Guo, M. S. Khan, W.-Y. Wong, P. R. Raithby, *Chem. Soc. Rev.* **2019**, *48*, 5547–5563.
[9] W.-Y. Wong, *Macromol. Chem. Phys.* **2008**, *209*, 14–24.
[10] C.-L. Ho, Z.-Q. Yu, W.-Y. Wong, *Chem. Soc. Rev.* **2016**, *45*, 5264–5295.
[11] C. Cebrián, M. Mauro, *Beilstein J. Org. Chem.* **2018**, *14*, 1459–1481.
[12] J. Kalinowski, V. Fattori, M. Cocchi, J. A. G. Williams, *Coord. Chem. Rev.* **2011**, *255*, 2401–2425.
[13] J. A. G. Williams, S. Develay, D. L. Rochester, L. Murphy, *Coord. Chem. Rev.* **2008**, *252*, 2596–2611.
[14] A. Colombo, C. Dragonetti, V. Guerchais, D. Roberto, *Coord. Chem. Rev.* **2021**, *446*, 214113.
[15] A. Fürstner, *Chem. Soc. Rev.* **2009**, *38*, 3208–3221.
[16] K. Sakai, H. Ozawa, *Coord. Chem. Rev.* **2007**, *251*, 2753–2766.
[17] Q. Dong, Z. Meng, C.-L. Ho, H. Guo, W. Yang, I. Manners, L. Xu, W.-Y. Wong, *Chem. Soc. Rev.* **2018**, *47*, 4934–4953.
[18] H. Yersin, in *Transition Metal and Rare Earth Compounds: Excited States, Transitions, Interactions III* (Ed.: H. Yersin), Springer Berlin Heidelberg, Berlin, Heidelberg, **2004**, pp. 1–26.
[19] H. Yersin, D. Donges, in *Transition Metal and Rare Earth Compounds: Excited States, Transitions, Interactions II* (Ed.: H. Yersin), Springer Berlin Heidelberg, Berlin, Heidelberg, **2001**, pp. 81–186.
[20] H. Yersin, A. F. Rausch, R. Czerwieniec, T. Hofbeck, T. Fischer, *Coord. Chem. Rev.* **2011**, *255*, 2622–2652.
[21] A. F. Rausch, L. Murphy, J. A. G. Williams, H. Yersin, *Inorg. Chem.* **2009**, *48*, 11407–11414.
[22] Z. Wang, E. Turner, V. Mahoney, S. Madakuni, T. Groy, J. Li, *Inorg. Chem.* **2010**, *49*, 11276–11286.
[23] J. A. G. Williams, in *Photochemistry and Photophysics of Coordination Compounds II* (Eds.: V. Balzani, S. Campagna), Springer Berlin Heidelberg, Berlin, Heidelberg, **2007**, pp. 205–268.
[24] M. Cocchi, D. Virgili, V. Fattori, D. L. Rochester, J. A. G. Williams, *Adv. Funct. Mater.* **2007**, *17*, 285–289.
[25] M. Cocchi, J. Kalinowski, V. Fattori, J. A. G. Williams, L. Murphy, *Appl. Phys. Lett.* **2009**, *94*, 073309.
[26] V. W.-W. Yam, R. P.-L. Tang, K. M.-C. Wong, K.-K. Cheung, *Organometallics* **2001**, *20*, 4476–4482.
[27] K. M.-C. Wong, V. W.-W. Yam, *Coord. Chem. Rev.* **2007**, *251*, 2477–2488.
[28] A. M. Prokhorov, T. Hofbeck, R. Czerwieniec, A. F. Suleymanova, D. N. Kozhevnikov, H. Yersin, *J. Am. Chem. Soc.* **2014**, *136*, 9637–9642.
[29] G. S.-M. Tong, C.-M. Che, *Chem. Eur. J.* **2009**, *15*, 7225–7237.
[30] X.-C. Hang, T. Fleetham, E. Turner, J. Brooks, J. Li, *Angew. Chem. Int. Ed.* **2013**, *52*, 6753–6756.
[31] Y. Chi, P.-T. Chou, *Chem. Soc. Rev.* **2010**, *39*, 638–655.
[32] S. C. Gangadharappa, I. Maisuls, D. A. Schwab, J. Kösters, N. L. Doltsinis, C. A. Strassert, *J. Am. Chem. Soc.* **2020**, *142*, 21353–21367.
[33] L. Mercs, M. Albrecht, *Chem. Soc. Rev.* **2010**, *39*, 1903–1912.
[34] M. Skander, P. Retailleau, B. Bourrié, L. Schio, P. Mailliet, A. Marinetti, *J. Med. Chem.* **2010**, *53*, 2146–2154.

[35] R. W.-Y. Sun, A. Lok-Fung Chow, X.-H. Li, J. J. Yan, S. S.-Y. Chui, C.-M. Che, *Chem. Sci.* **2011**, *2*, 728–736.
[36] S. Harlepp, E. Chardon, M. Bouché, G. Dahm, M. Maaloum, S. Bellemin-Laponnaz, *Int. J. Mol. Sci.* **2019**, *20*, 4198.
[37] R. Visbal, M. C. Gimeno, *Chem. Soc. Rev.* **2014**, *43*, 3551–3574.
[38] J. Friedel, M. Krause, R. Jordan, I. Maisuls, D. Brünink, D. Schwab, N. L. Doltsinis, C. A. Strassert, A. Klein, *Molecules* **2022**, *27*, 8054.
[39] T. Zou, C.-N. Lok, Y. M. E. Fung, C.-M. Che, *Chem. Commun.* **2013**, *49*, 5423–5425.
[40] F. Wurl, S. Stipurin, J. I. Kollar, T. Strassner, *Angew. Chem. Int. Ed.* **2023**, *62*, e202301225.
[41] S. Stipurin, T. Strassner, *Eur. J. Inorg. Chem.* **2022**, *2022*, e202200295.
[42] T. Strassner, *Acc. Chem. Res.* **2016**, *49*, 2680–2689.
[43] P. Pinter, J. Soellner, T. Strassner, *Eur. J. Inorg. Chem.* **2021**, *2021*, 3104–3107.
[44] B. Schulze, C. Friebe, M. Jäger, H. Görls, E. Birckner, A. Winter, U. S. Schubert, *Organometallics* **2018**, *37*, 145–155.
[45] A. R. Naziruddin, C.-S. Lee, W.-J. Lin, B.-J. Sun, K.-H. Chao, A. H. H. Chang, W.-S. Hwang, *Dalton Trans.* **2016**, *45*, 5848–5859.
[46] G. Li, S. Liu, Y. Sun, W. Lou, Y.-F. Yang, Y. She, *J. Mater. Chem. C* **2022**, *10*, 210–218.
[47] K. Li, G. Cheng, C. Ma, X. Guan, W.-M. Kwok, Y. Chen, W. Lu, C.-M. Che, *Chem. Sci.* **2013**, *4*, 2630–2644.
[48] H. Wang, B. Zhang, X. Yan, S. Guo, *Dalton Trans.* **2018**, *47*, 528–537.
[49] R. Maity, B. Sarkar, *JACS Au* **2022**, *2*, 22–57.
[50] P. Anastas, J. C. Warner, *Green Chemistry: Theory and Practice*, Oxford University Press, New York, **1998**.
[51] L. Benhamou, E. Chardon, G. Lavigne, S. Bellemin-Laponnaz, V. César, *Chem. Rev.* **2011**, *111*, 2705–2733.
[52] M. Hans, J. Lorkowski, A. Demonceau, L. Delaude, *Beilstein J. Org. Chem.* **2015**, *11*, 2318–2325.
[53] R. Petrucci, M. Feroci, L. Mattiello, I. Chiarotto, *Mini-Rev. Org. Chem.* **2021**, *18*, 27–42.
[54] Coffee consumption worldwide from 2012/13 to 2020/21. https://www.statista.com/statistics/292595/global-coffee-consumption/ (last accessed: 2023-10-10).
[55] B. Dockendorff, D. A. Holman, G. D. Christian, J. Ruzicka, *Anal. Commun.* **1998**, *35*, 357–359.
[56] M. D. A. Saldaña, R. S. Mohamed, M. G. Baer, P. Mazzafera, *J. Agric. Food Chem.* **1999**, *47*, 3804–3808.
[57] S. Machmudah, K. Kitada, M. Sasaki, M. Goto, J. Munemasa, M. Yamagata, *Ind. Eng. Chem. Res.* **2011**, *50*, 2227–2235.
[58] A. Vandeponseele, M. Draye, C. Piot, G. Chatel, *Clean Technol.* **2021**, *3*, 335–350.
[59] H. Valdés, D. Canseco-González, J. M. Germán-Acacio, D. Morales-Morales, *J. Organomet. Chem.* **2018**, *867*, 51–54.
[60] F. Mazars, L. Delaude, *Organometallics* **2023**, *42*, 1589–1597.
[61] O. Bysewski, A. Winter, U. S. Schubert, *Inorganics* **2023**, *11*, 164.
[62] M. M. Rahman, J. Zhang, Q. Zhao, J. Feliciano, E. Bisz, B. Dziuk, R. Lalancette, R. Szostak, M. Szostak, *Organometallics* **2022**, *41*, 2281–2290.
[63] F.-T. Luo, H.-K. Lo, *J. Organomet. Chem.* **2011**, *696*, 1262–1265.
[64] D. Meng, D. Li, T. Ollevier, *RSC Adv.* **2019**, *9*, 21956–21963.
[65] J. J. Hu, S.-Q. Bai, H. H. Yeh, D. J. Young, Y. Chi, T. S. A. Hor, *Dalton Trans.* **2011**, *40*, 4402–4406.
[66] T. M. Kirse, J. Lüke, I. Maisuls, A. Hepp, C. A. Strassert, *Photochem. Photobiol.* **2023**, *99*, 616–623.
[67] O. Bysewski, A. Winter, P. Liebing, U. S. Schubert, *Molecules* **2022**, *27*, 4316.
[68] Mercury v2022.3.0.
[69] M. Krause, I. Maisuls, S. Buss, C. A. Strassert, A. Winter, U. S. Schubert, S. S. Nair, B. Dietzek-Ivanšić, A. Klein, *Molecules* **2022**, *27*, 7022.
[70] M. D. Weber, M. Viciano-Chumillas, D. Armentano, J. Cano, R. D. Costa, *Dalton Trans.* **2017**, *46*, 6312–6323.
[71] A. Lüning, J. Schur, L. Hamel, I. Ott, A. Klein, *Organometallics* **2013**, *32*, 3662–3672.
[72] P. R. Murray, S. Crawford, A. Dawson, A. Delf, C. Findlay, L. Jack, E. J. L. McInnes, S. Al-Musharafi, G. S. Nichol, I. Oswald, L. J. Yellowlees, *Dalton Trans.* **2012**, *41*, 201–207.
[73] M. Hissler, W. B. Connick, D. K. Geiger, J. E. McGarrah, D. Lipa, R. J. Lachicotte, R. Eisenberg, *Inorg. Chem.* **2000**, *39*, 447–457.
[74] T. Eskelinen, S. Buss, S. K. Petrovskii, E. V. Grachova, M. Krause, L. Kletsch, A. Klein, C. A. Strassert, I. O. Koshevoy, P. Hirva, *Inorg. Chem.* **2021**, *60*, 8777–8789.
[75] L. Kletsch, R. Jordan, A. S. Köcher, S. Buss, C. A. Strassert, A. Klein, *Molecules* **2021**, *26*, 5051.
[76] J. A. Therrien, M. O. Wolf, B. O. Patrick, *Dalton Trans.* **2018**, *47*, 1827–1840.
[77] S. Y.-L. Leung, E. S.-H. Lam, W. H. Lam, K. M.-C. Wong, W.-T. Wong, V. W.-W. Yam, *Chem. Eur. J.* **2013**, *19*, 10360–10369.
[78] M. Bachmann, D. Suter, O. Blacque, K. Venkatesan, *Inorg. Chem.* **2016**, *55*, 4733–4745.
[79] W. Lu, B.-X. Mi, M. C. W. Chan, Z. Hui, C.-M. Che, N. Zhu, S.-T. Lee, *J. Am. Chem. Soc.* **2004**, *126*, 4958–4971.
[80] T. Liska, A. Swetz, P.-N. Lai, M. Zeller, T. S. Teets, T. G. Gray, *Chem. Eur. J.* **2020**, *26*, 8417–8425.
[81] S. J. Farley, D. L. Rochester, A. L. Thompson, J. A. K. Howard, J. A. G. Williams, *Inorg. Chem.* **2005**, *44*, 9690–9703.
[82] M. Li, T. Liska, A. Swetz, N. Ayoub, P.-N. Lai, M. Zeller, T. G. Gray, *Organometallics* **2020**, *39*, 1667–1671.
[83] M. Stephenson, C. Reichardt, M. Pinto, M. Wächtler, T. Sainuddin, G. Shi, H. Yin, S. Monro, E. Sampson, B. Dietzek, S. A. McFarland, *J. Phys. Chem. A* **2014**, *118*, 10507–10521.
[84] F. Neese, F. Wennmohs, U. Becker, C. Riplinger, *J. Chem. Phys.* **2020**, *152*.
[85] F. Neese, *WIREs Comput. Mol. Sci.* **2022**, *12*, e1606.
[86] F. Weigend, R. Ahlrichs, *Phys. Chem. Chem. Phys.* **2005**, *7*, 3297–3305.
[87] A. D. Becke, *Phys. Rev. A* **1988**, *38*, 3098–3100.
[88] J. P. Perdew, W. Yue, *Phys. Rev. B* **1986**, *33*, 8800–8802.
[89] S. Grimme, J. Antony, S. Ehrlich, H. Krieg, *J. Chem. Phys.* **2010**, *132*.
[90] S. Grimme, S. Ehrlich, L. Goerigk, *J. Comput. Chem.* **2011**, *32*, 1456–1465.
[91] V. Barone, M. Cossi, *J. Phys. Chem. A* **1998**, *102*, 1995–2001.
[92] M. Cossi, N. Rega, G. Scalmani, V. Barone, *J. Comput. Chem.* **2003**, *24*, 669–681.
[93] C. Lee, W. Yang, R. G. Parr, *Phys. Rev. B* **1988**, *37*, 785–789.
[94] A. D. Becke, *J. Chem. Phys.* **1992**, *96*, 2155–2160.
[95] Chemcraft – graphical software for visualization of quantum chemistry computations. Version 1.8, build 682. https://www.chemcraftprog.com.
[96] S. Preus, DecayFit – Fluorescence Decay Analysis Software, v1.3, Fluor Tools, **2014**, https://www.fluortools.com.

Manuscript received: October 15, 2023
Revised manuscript received: December 15, 2023
Accepted manuscript online: December 27, 2023
Version of record online: January 10, 2024